

# Design, synthesis, and preliminary in vitro and in silico antiviral activity of [4,7]phenantrolines and 1-oxo-1,4-dihydro-[4,7]phenantrolines against single-stranded positive-sense RNA genome viruses

Antonio Carta,<sup>a,\*</sup> Mario Loriga,<sup>a</sup> Giuseppe Paglietti,<sup>a</sup> Marco Ferrone,<sup>b</sup> Maurizio Fermeglia,<sup>b</sup> Sabrina Pricl,<sup>b</sup> Tiziana Sanna,<sup>c</sup> Cristina Ibba,<sup>c</sup> Paolo La Colla<sup>c,\*</sup> and Roberta Loddo<sup>c</sup>

<sup>a</sup>Dipartimento Farmaco Chimico Tossicologico, Università degli Studi di Sassari, Via Muroni 23/a, 07100 Sassari, Italy

<sup>b</sup>Laboratorio MOSE, Dipartimento di Ingegneria Chimica, dell'Ambiente e delle Materie Prime, Università degli Studi di Trieste, Piazzale Europa 1, 34127 Trieste, Italy

<sup>c</sup>Dipartimento di Scienze e Tecnologie Biomediche, Sezione di Microbiologia e Virologia Generale e Biotecnologie Microbiche, Università degli Studi di Cagliari, Cittadella Universitaria, S.S. 554, Km 4500, 09042 Monserrato (Ca), Italy

Received 22 May 2006; revised 4 January 2007; accepted 4 January 2007

Available online 9 January 2007

**Abstract**—Following the antiviral screening of a wide series of new angular and linear *N*-tricyclic systems both in silico and in vitro, the [4,7]phenantroline nucleus emerged as a new ring system endowed with activity against viruses containing single-stranded, positive-sense RNA genomes (ssRNA<sup>+</sup>). Here, we report our new pathway to the synthesis of this nucleus and of several related derivatives, as well as the results of both cell-based antiviral assays and molecular dynamics simulations. In the antiviral screening, several compounds (**9** and **16–20**) showed to be fairly active against BVDV, CVB-2, and Polio 1 (EC<sub>50</sub>, 6–25 μM). According to molecular dynamics simulations, compounds (**15**) and (**17**) emerged for its potency against the HCV NS5B, with a calculated IC<sub>50</sub> of 11–12 μM.

© 2007 Elsevier Ltd. All rights reserved.

## 1. Introduction

Viruses belonging to the *Flaviviridae* family have a single-stranded, positive-sense RNA genome (ssRNA<sup>+</sup>)<sup>1</sup> and cause clinically significant diseases in humans and animals. This virus family includes three genera, i.e., *Pestivirus* (i.e., bovine viral diarrhoea virus [BVDV]), *Flavivirus* (i.e., yellow fever [YFV], dengue, and West Nile viruses), and *Hepacivirus* (Hepatitis C virus [HCV]).

HCV is a major cause of human hepatitis, globally.<sup>2</sup> The World Health Organization (WHO) estimates that over

170 million people worldwide are presently infected with this virus.<sup>3</sup> Most infections become persistent, and about 60% of cases progress toward chronic liver disease, which in turn, can lead to development of cirrhosis, hepatocellular carcinoma, and liver failure.<sup>4,5</sup> Actually, with the exception of YFV, no vaccine exists against the various *Flaviviridae* members; therefore, new therapies and preventative agents are strongly needed.

Other important ssRNA<sup>+</sup> viruses are those belonging to the *Picornaviridae* family. These viruses cause a variety of illnesses, including meningitis, cold, heart infection, conjunctivitis, and hepatitis<sup>6</sup>. This family includes nine genera, some of which comprise major human pathogens, namely, *Enterovirus* (including *Poliovirus*, *Coxsackievirus*, *Echovirus*), *Rhinovirus* (approximately 105 serotypes), and *Hepatovirus* (Hepatitis A virus [HAV]). At present, no specific antiviral therapy is available for the treatment of *Picornaviridae* infections.

**Keywords:** [4,7]Phenantrolines; ssRNA<sup>+</sup>; RNA-dependent RNA-polymerase; HCV NS5B; Pestiviruses; Flaviviruses; Enteroviruses; Molecular dynamics simulations.

\* Corresponding authors. Tel.: +39 079228722; fax: +39 07922820; e-mail addresses: [acarta@uniss.it](mailto:acarta@uniss.it); [placolla@unica.it](mailto:placolla@unica.it)

As part of our antiviral research program, we have recently synthesized and tested *in vitro* a series of new angular and linear *N*-tricyclic systems against representatives of the above-cited ssRNA<sup>+</sup> viruses. Further we tested these compounds for activity against viruses representative of an additional genus of ssRNA<sup>+</sup> genomes [Human immunodeficiency virus (HIV-1)], of double-stranded RNA genomes (dsRNA) [*Reovirus* (Reo-1)], and of single-stranded, negative-sense RNA genomes (ssRNA<sup>-</sup>) [respiratory syncytial virus (RSV) and vesicular stomatitis virus (VSV)]. Interestingly, [4,7]phenantrolines were found to be endowed with inhibitory activity against members of the *Flaviviridae* and *Picornaviridae* families.

In the light of some similarities between a number of our active compounds and the nonnucleoside proprietary inhibitor ((2*S*)-2-[(2,4-dichloro-benzoyl)-(3-trifluoromethyl-benzyl)-amino]-3-phenyl-propionic acid)<sup>7</sup> (hereafter named **Shire A**, see Fig. 1) targeting the HCV NS5B, we considered that this enzyme could also be the target of title compounds. Thus, the *in silico*

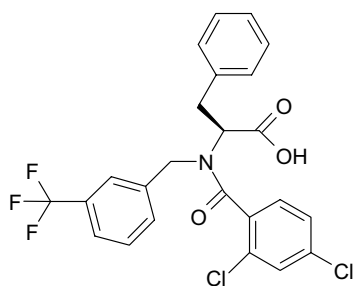


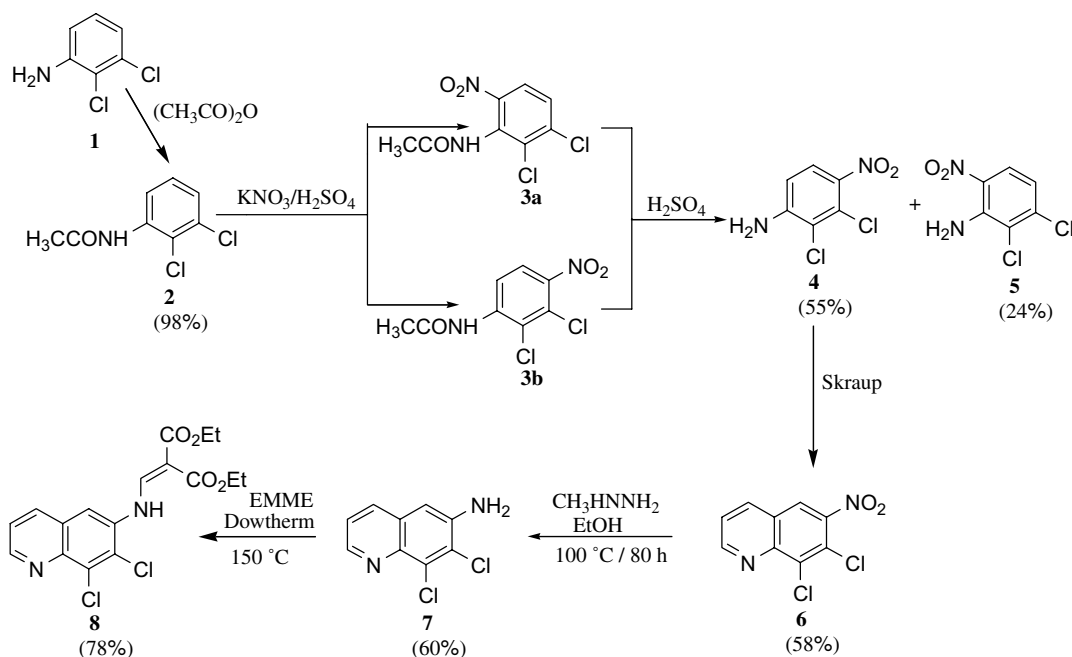
**Figure 1.** Chemical structure of ((2*S*)-2-[(2,4-dichloro-benzoyl)-(3-trifluoromethyl-benzyl)-amino]-3-phenyl-propionic acid or **Shire A**), a proprietary nonnucleoside inhibitor of HCV NS5B.<sup>7</sup>

interactions between the latter and the HCV NS5B were studied in detail, the relevant free energies of binding  $\Delta G_{\text{bind}}$  calculated, and the corresponding IC<sub>50</sub> values predicted accordingly.

The [4,7]phenantroline nucleus is known since 1909<sup>8</sup> and some of its derivatives have been subsequently described.<sup>9</sup> Here, we report a new pathway for the synthesis of this nucleus and of related derivatives. Substituents at position 1 (chloro, alkoxy, amino) were chosen in order to verify whether they were able to either improve or direct the activity against specific viruses. 1-Oxo-[4,7]phenantroline derivatives were necessary intermediates of the reaction, and they were also tested for biological activity. In addition, we evaluated the influence on the antiviral activity of chlorine atoms at positions 5 and 6.

## 2. Chemistry

The synthesis of key intermediates 6-amino-7,8-dichloroquinoline (**7**) and diethyl 2-[(7,8-dichloroquinol-6-ylamino)-methylene]malonate (**8**) is outlined in Scheme 1. The synthetic route of (**7**) was modified according to a procedure previously described by some of us.<sup>10</sup> The mixture of regioisomers (**3a** and **3b**) obtained by nitration of the acetanilide (**2**) at 2–5 °C was hydrolyzed with concentrated sulfuric acid, yielding the corresponding mixture of anilines (**4** and **5**). Chromatographic separation afforded the desired aniline (**4**). The nitroquinoline (**6**) was in turn obtained via Skraup synthesis starting from (**4**).<sup>10</sup> Finally, the known aminoquinoline (**7**) was obtained in 60% yield by reduction of (**6**) with methylhydrazine in ethanol, heated in a sealed steel vessel at 100 °C for 65 h. The same reaction performed with hydrazine hydrate (99%) in ethanol at 160 °C (in sealed



**Scheme 1.** Synthetic pathway for key quinoline intermediates **7** and **8**.

steel vessel) for 10 h afforded the aminoquinoline (**7**) in lower yield (50%).<sup>10</sup> This new procedure allowed improving the total yield of the five steps (19% against 11%) necessary to obtain compound (**7**). The second key intermediate (**8**) was obtained in good yield (78%), according to a described procedure,<sup>11</sup> by reaction of (**7**) with diethyl ethoxymethylenemalonate (EMME) in Dowtherm (mixture of biphenyl and phenyl ether in 26.5:73.5 ratio) at 150 °C.

The syntheses of all target compounds are outlined in Schemes 2–4. In general, [4,7]phenantroline and all its new derivatives (**9–20**) were obtained in good yields (51–94%). 5,6-Dichlorophenantroline (**9**), and its known unsubstituted nucleus (**10**),<sup>8</sup> was prepared submitting the amine (**7**) to Skraup reaction, followed by dehalogenation with hydrazine and palladium–charcoal in ethanol heating in a sealed steel vessel at 100 °C for 2.5 h (yields of 86% and 54%, respectively) (Scheme 2).

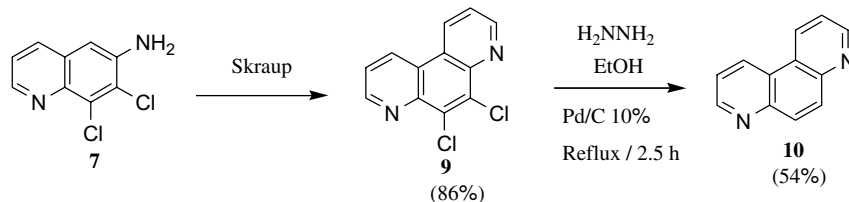
Preparation of 1-oxo-1,4-dihydro-[4,7]phenantrolines is summarized in Scheme 3. Intermediate (**8**) underwent ring closure in Dowtherm at 250 °C for 2 h, giving rise to the expected 1-oxo-[4,7]phenantroline (**11**) (51% yield), accompanied by its decarboxylation product (**12**) (20% yield). Compound (**12**) was also obtained alone carrying out the same reaction for a longer time (15 h, 69% yield). Finally, we observed that heating

the ester (**11**) at 250 °C for 12 h resulted in compound hydrolysis followed by decarboxylation, and yielded **12** in 81% yield. Acid hydrolysis of (**11**) gave the acid (**13**) in 91% yield. Known derivative (**14**)<sup>9a</sup> was finally obtained carrying out the dehalogenation of **12** (56% yield) with hydrazine and palladium–charcoal, as described above.

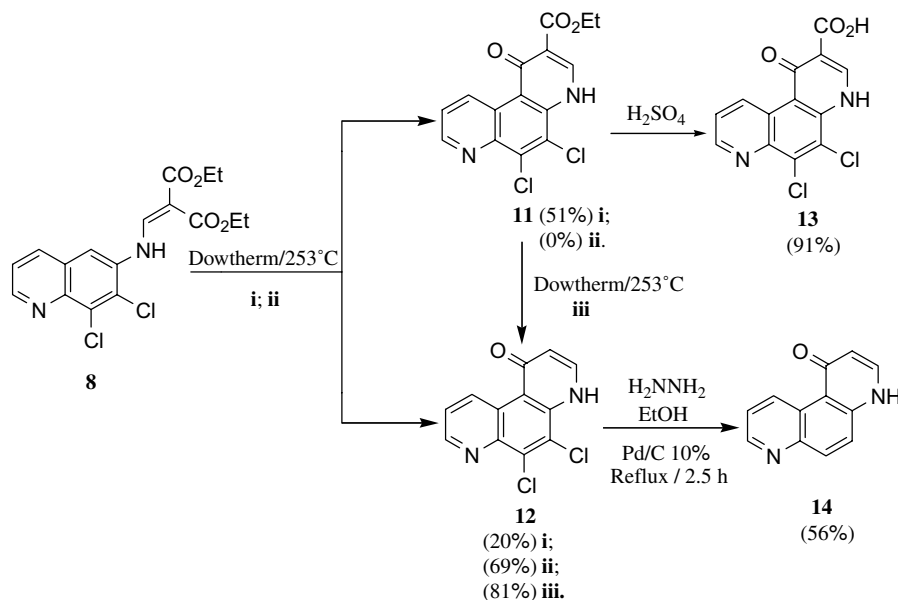
The synthesis of 1-substituted-[4,7]phenantrolines is shown in Scheme 4. Ethylation with diethyl sulfate on (**12**) occurred at the oxygen to give the ethoxy derivative (**16**) (72% yield), whereas chlorination with POCl<sub>3</sub> led to the trichlorophenantroline (**15**) (72% yield). The latter compound, after nucleophilic displacement by ammonia, yielded the corresponding aminophenantroline (**18**) (85% yield) that, after acetylation with acetic anhydride, gave (**20**) in 78% yield. Finally, dehalogenation of (**18**) was carried out as reported above producing (**19**) in 94% yield.

### 3. Virology and molecular modeling

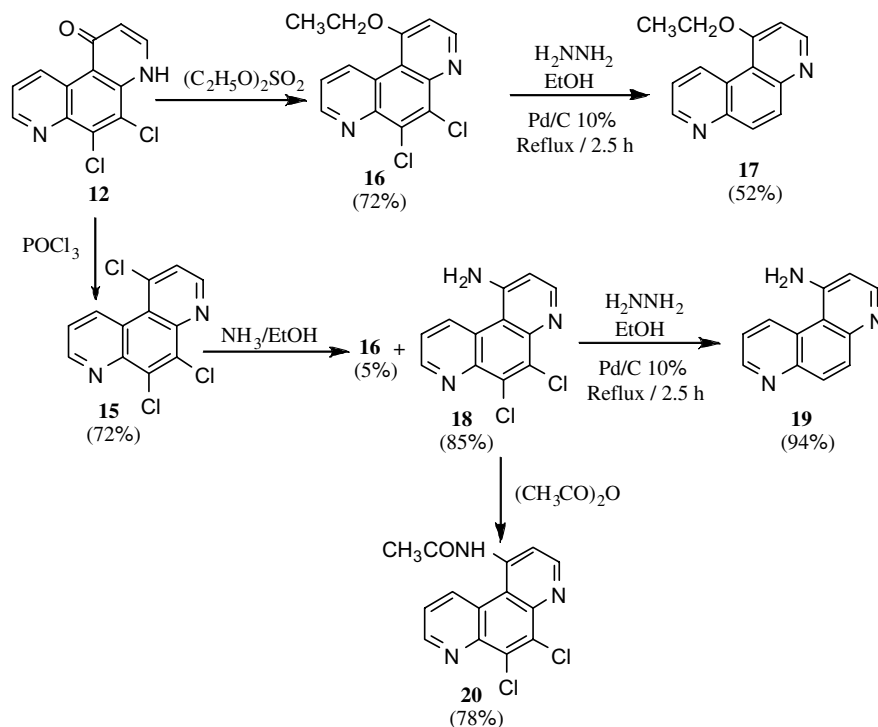
Title compounds (**9–20**) were evaluated in vitro against ssRNA<sup>+</sup> viruses representative of the *Flaviviridae* and *Picornaviridae* families. In particular, viruses representative of two of the three genera of the *Flaviviridae* family, i.e., YFV (*Flaviviruses*) and BVDV (*Pestiviruses*), and of one genus of the *Picornaviridae* family: CVB-2 and Polio



Scheme 2. Synthetic pathway for [4,7]-phenantroline nucleus and its 5,6-dichloroderivative.



Scheme 3. Synthetic pathway for 1-oxo-[4,7]-phenantroline nucleus and some of its derivatives. (i) 2 h; (ii) 15 h; (iii) 13 h.



**Scheme 4.** Synthetic pathway for 1-substituted-[4,7]-phenantrolines.

1 (*Enteroviruses*) were tested. Compounds were also tested against an additional ssRNA<sup>+</sup> virus [Human immunodeficiency virus (HIV-1)], and representatives of dsRNA viruses [*Reoviridae* (Reo-1)] and ssRNA<sup>-</sup> viruses [respiratory syncytial virus (RSV) and vesicular stomatitis virus (VSV)]. Due to the lack of efficient cell

culture systems for the multiplication of HCV, title compounds were evaluated in silico against the most probable HCV target protein, i.e., the RNA-dependent RNA-polymerase. All compounds were modeled and docked into the protein, following an ad hoc developed procedure. The corresponding free energies of binding,

**Table 1.** Cytotoxicity and antiviral activity of [4,7]phenantrolines (**9**, **10**, and **15–20**) and 1-oxo-1,4-dihydro-[4,7]phenantrolines (**11–14**) against ssRNA<sup>+</sup> viruses

Compound	<i>Pestiviruses</i>			<i>Flaviviruses</i>		<i>Enteroviruses</i>			<i>Retroviruses</i>							
	<sup>a</sup> CC <sub>50</sub>	<sup>e</sup> MDBK	<sup>b</sup> EC <sub>50</sub>	BVDV	<sup>a</sup> CC <sub>50</sub>	<sup>f</sup> BHK	<sup>c</sup> EC <sub>50</sub>	YFV	<sup>a</sup> CC <sub>50</sub>	<sup>g</sup> Vero	<sup>c</sup> EC <sub>50</sub>	CVB-2	<sup>c</sup> EC <sub>50</sub>	Sb-1	<sup>d</sup> CC <sub>50</sub>	<sup>e</sup> EC <sub>50</sub>
															<sup>h</sup> MT-4	HIV-1
<b>9</b>	>100		<b>16</b>		>100		>100		25		<b>11</b>		<b>6</b>		24	>24
<b>10</b>	>100		<b>17</b>		>100		>100		80		>80		>80		61	>61
<b>11</b>	>100		<b>35</b>		25		>25		90		>90		>90		32	>32
<b>12</b>	>100		<b>16</b>		>100		>100		80		>80		>80		47	>47
<b>13</b>	>100		>100		23		>23		100		>100		85		>100	>100
<b>14</b>	>100		95		66		>66		>100		>100		>100		>100	>100
<b>15</b>	54		>54		>100		>100		>100		>100		>100		6.4	>6.4
<b>16</b>	64		<b>25</b>		25		>25		75		<b>2</b>		<b>11</b>		>100	>100
<b>17</b>	64		<b>6</b>		35		>35		80		<b>5</b>		<b>17</b>		56	>56
<b>18</b>	24		≥24		11		>11		40		<b>2</b>		<b>14</b>		7.2	>7.2
<b>19</b>	63		<b>9</b>		>100		>100		90		>90		>90		50	>50
<b>20</b>	32		<b>22</b>		18		>18		50		<b>2</b>		<b>21</b>		13	>13

<sup>a–d</sup>Data represent mean values for three independent determinations. Variation among duplicate samples was less than 15%. Interesting antiviral activity values have been highlighted in bold for convenience.

<sup>a</sup>Compound concentration (μM) required to reduce the viability of mock-infected cells by 50%, as determined by the MTT method, or the confluence of the monolayer, as determined by methylene blue staining.

<sup>b</sup>Compound concentration (μM) required to achieve 50% protection from virus-induced cytopathogenicity, as determined by the MTT method.

<sup>c</sup>Compound concentration (μM) required to reduce the virus plaque number by 50%.

<sup>d</sup>Compound concentration (μM) required to reduce cell proliferation by 50%, as determined by the MTT method, under conditions allowing untreated controls to undergo at least three consecutive rounds of multiplication.

<sup>e</sup>Madin Darby bovine kidney.

<sup>f</sup>Baby hamster kidney.

<sup>g</sup>Monkey kidney.

<sup>h</sup>CD4<sup>+</sup> human T-cells.

as well as the estimated  $IC_{50}$ , were then calculated from molecular dynamics (MD) simulations.

#### 4. Results and discussion

[4,7]Phenantrolines (**9**, **10**, and **15–20**) and 1-oxo-[4,7]-phenantrolines (**11–14**) were evaluated in parallel cell-based assays for cytotoxicity and antiviral activity (Table 1). Different compounds exhibited different cytotoxicity for different cell lines. Compounds **18** and **20** turned out to be the most cytotoxic for all the cell lines used in this study. On the other hand, compound **9** was slightly cytotoxic for Vero and MT-4, compound **11** for BHK and MT-4, compounds **13**, **16**, and **17** for BHK, whereas compound **15** was the most cytotoxic for MT-4 cell lines.

As far as the antiviral activity is concerned, title phenantrolines can be divided into derivatives devoid of (**10**, **14**, **17**, and **19**) or characterized by (**9**, **11–13**, **15**, **16**, **18**, and **20**) the 5,6-dichloro substituent. With the due exceptions, the former are specifically active against the *Pestivirus* representative, whereas the latter are more broadly active against *Pesti* and *Enterovirus* representatives. None of title compounds, however, turned out active against YFV, HIV-1 or representatives of dsRNA (Reo) and ssRNA<sup>-</sup> viruses (RSV or VSV) (data not shown).

Among the phenantrolines devoid of the 5,6 dichloro substituent (**10**, **14**, **17**, and **19**), compounds **10** and **19** turned out to be selective inhibitors of BVDV in the range 9–17  $\mu$ M, whereas **14** was inactive and **17** was active but not selective. The lack of the two chlorine atoms correlates with a specific activity against BVDV, provided that position 1 is unsubstituted (**10**) or substituted with amino (**19**) groups. In fact, when oxygen (**14**) is present at this position, the antiviral activity is lost. The reason why **17** is both potently active against *Enteroviruses* and BVDV is not immediately evident (Further studies are in progress).

Among 5,6-dichloro-phenantrolines (**9**, **11**, **12**, **13**, **15**, **16**, **18**, and **20**), derivatives **9**, **16**, **18**, and **20** inhibited CVB-2, Polio 1, and BVDV at concentrations ranging from 2 to 11, 6 to 21, and 16 to 25, respectively, even if in a few cases some  $EC_{50}$  are close to  $CC_{50}$ . On the other hand, the remaining compounds were inactive against the enteroviruses and only **11** and **12** showed activity against BVDV.

SAR studies suggest that the presence of a 5,6-dichloro substituent correlates with the broad spectrum activity of phenantrolines **9**, **16**, **18**, and **20**, which is characterized by a higher potency and selectivity against Coxsackie B-2 provided that position 1 is unsubstituted (**9**) or substituted with alkoxy (**16**), amino (**18**) or acetylamino (**20**) groups. In fact, when oxygen (1-oxo-[4,7]phenantrolin derivatives **11–13**) or chlorine (1-chloro-[4,7]phenantrolin **15**) is present at this position, the antiviral activity is lost. The reason why **11** and **12** maintain some anti-BVDV activity is not immediately evident.

As outlined before, these in vitro tests were paralleled by in silico experiments. In general, there are two key requirements for the computer-aided structure-based

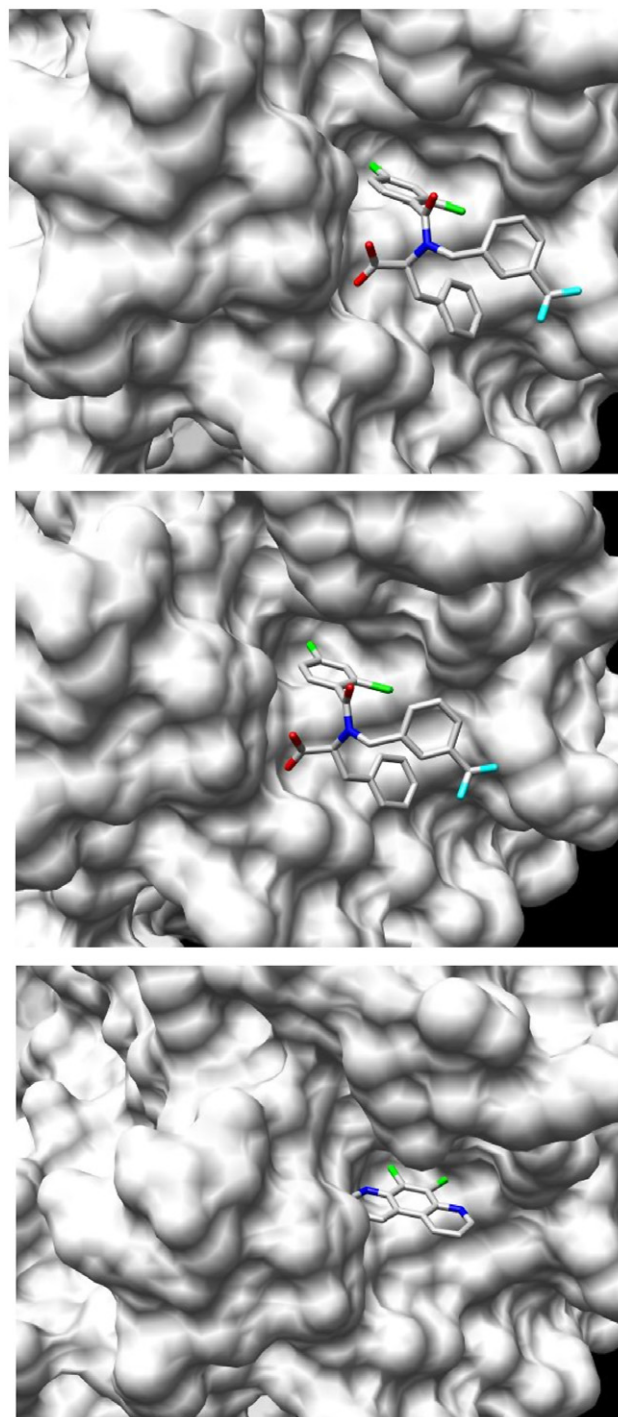


**Figure 2.** (a, top) Comparison between the co-crystallized conformation of inhibitor **Shire A** into the allosteric binding site of HCV NS5B; (b, middle) the corresponding docked conformation, and (c, bottom) binding mode of compound (**9**) in the same enzyme pocket. Models in Figure 1b and c were obtained upon application of the computational strategy adopted in this work. The inhibitor molecules are shown as a stick model, and the atom color-coding is as follows: carbon, gray; nitrogen, blue, oxygen, red; fluorine, cyan; and chlorine, green. Hydrogen atoms and water molecules are omitted for clarity.

drug design methods: correctly generating conformations of docked ligands and accurately predicting the binding affinity. Accordingly, as a preliminary test, we modeled, docked, and calculated the free energy of binding (and the corresponding  $IC_{50}$  values) for the proprietary inhibitors of HCV NS5B **Shire A**, for which both the crystallographic structures of the relevant RdRp complex and the corresponding  $IC_{50}$  value were available.<sup>7</sup> This was basically done by removing the inhibitor

from the enzyme allosteric site, building a new molecular model for this compound, applying the conformational procedure described in details in the Section 6 for the phenantroline derivatives, and finally docking it back into the NS5B surface pocket. The best docked structure, which is the configuration with the lowest docking energy in a prevailing cluster, was then compared with the corresponding crystal structure. Figure 2a and b shows a comparison between the

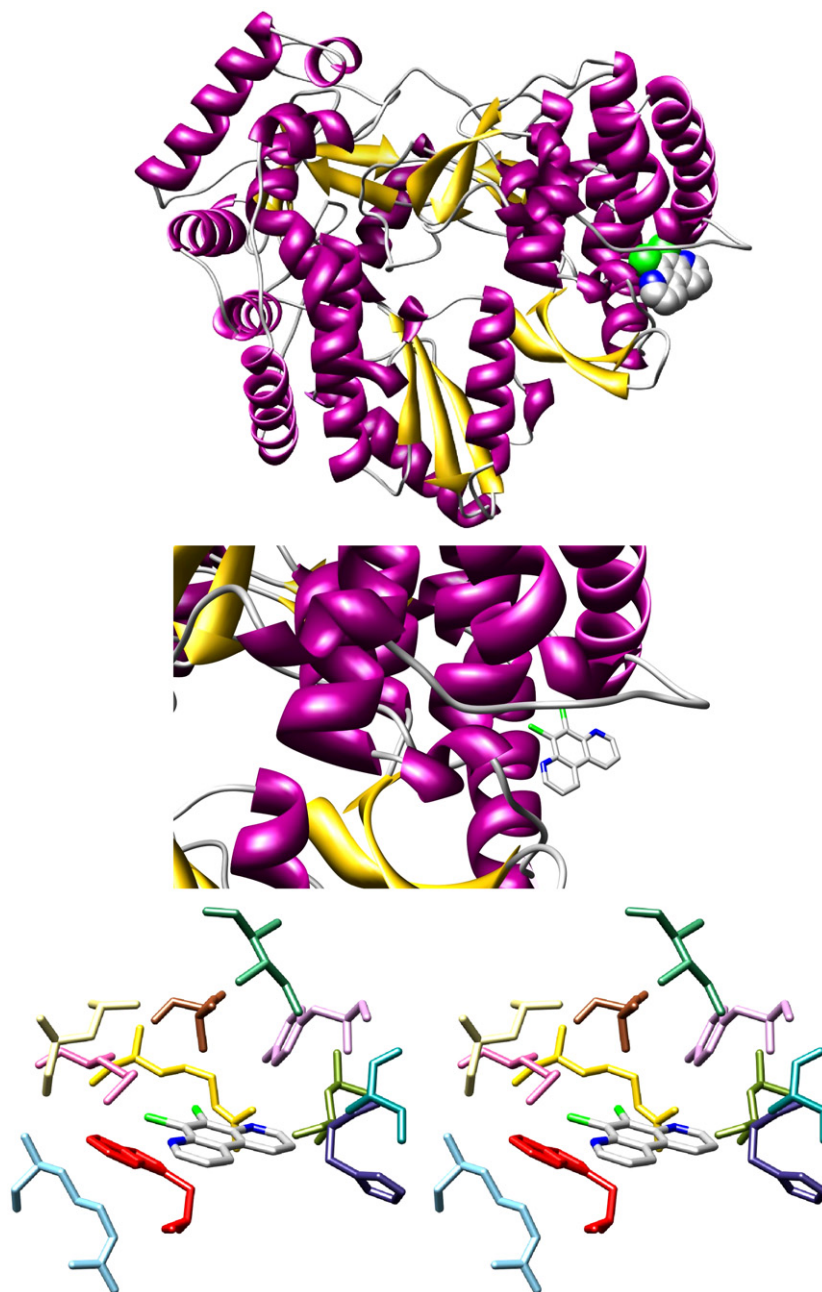


**Figure 3.** (a, top) Ribbon diagram of HCV NS5B/compound (**9**) complex structure as resulting from the applied docking/MD procedure. The protein is colored according to its secondary structure:  $\alpha$ -helices, purple;  $\beta$ -sheets, gold; turns and coils, light gray. The inhibitor (**9**) is represented as a CPK model with carbons in gray, nitrogens in blue, and chlorines in green. (b, middle) Detail of compound (**9**) (in a stick representation) in the binding pocket in the enzyme thumb subdomain. Color scheme as above. (c, bottom) A stereo view of the inhibitor-binding site of HCV NS5B/(**9**) complex. The inhibitor molecule is shown as a stick model (color scheme as above). The side chains of all residues that form the primary binding pocket interacting with compound (**9**) are shown as stick models, and the atom color-coding is as follows: L419, brown; R422, gold; M423, hot pink; L474, olive green; H475, dark slate blue; S476, dark cyan; Y477, plum; I482, sea green; L497, kaki; R501, sky blue; W528, red. Hydrogen atoms and water molecules are omitted for clarity.

co-crystallized conformation of inhibitor **Shire A** into the allosteric binding site of NS5B and the docked conformation obtained upon application of the computational strategy adopted in this work. At a first glance it can be seen that the agreement between the two structures is excellent. Further, the root-mean-square deviation (RMSD) between the docked configuration and the relevant crystal structures of this test inhibitor is equal to 0.01 Å. In the light of these blank-test results, and of the fact that this computational procedure was already successfully applied by us to predict the anti-HCV activity of other allosteric inhibitors of HCV NS5B,<sup>12</sup> the conceived modeling/docking procedure was applied for predicting the binding mode of the phenantroline derivatives in the HCV nonnucleoside binding site targeted by *Shire A*. Figure 2c illustrates, as an example, compound **9** docked into the HCV NS5B allosteric binding site.

This phenantroline derivative occupies the central portion of the polymerase extended allosteric cleft (see Fig. 3a and b), and the detailed interactions between **9** and the enzyme are shown in Figure 3c. The bottom of the binding pocket is formed by the main-chain atoms and the side chains of R501, W528, and H475, whilst the surrounding walls are formed by the side chains of R422, M423, L474, S476, and Y477. Finally, residues L497, L419, and I482 enclose the inhibitor from top (see Fig. 3c). As results from the inspection of the relevant HCV NS5B/**9** complex MD trajectory, this inhibitor makes a series of hydrophobic and van der Waals interactions with the residues lining the allosteric binding pocket in the enzyme. However, one of the most important interactions is a dual hydrogen bond that the positively charged guanidinium group of R422 forms with one of the heterocyclic nitrogen atoms of the inhibitor on one side (average dynamic length (ADL) = 2.7 Å), and with oxygen of the main-chain CO group of L474 on the other (ADL = 2.3 Å). The dichlorophenyl ring of **9** has extensive favorable interactions with at least seven residues. Topical van der Waals

and hydrophobic interactions are exchanged with the side chains of L419, M423, Y477, L474, H475, and W528. In addition, the same charged side chain of R422 contributes to screen the electronegative chlorine atoms, whilst the positive partial charges on the edges of the same aromatic ring bearing the halogen substituents are counterbalanced by the carbonyl oxygen atoms of L497 and F472, thus yielding favorable electrostatic stabilization to the complex.

In analogy with the nonnucleoside inhibitor **Shire A**, one of the heterocyclic rings and part of the unsubstituted side of inhibitor **9** basically float above the protein surface without making any strong interaction with the enzyme (see Fig. 2c). By inducing a rigid constraint to the entire molecular structure, however, the third condensed ring may contribute to a global conformation that is favorable to the protein/small molecule interaction.

The success of docking molecules into a target site is ultimately dependent, however, on the accuracy of the scoring function that ranks the compounds or, better, how well the corresponding binding affinities can be predicted. Ligand binding is governed by kinetic and thermodynamic principles. Factors that contribute to ligand binding include the hydrophobic effect, van der Waals interactions, hydrogen bonding, other electrostatic interactions, solvation, and entropic effects. If the change in free energy associated with complex formation is negative, the association will be favorable. Thus, once a candidate ligand is constructed, its interaction energy with its target protein is calculated and compared with that for other existing ligands. Accordingly, the last row of Table 2 reports the binding free energy  $\Delta G_{\text{bind}}$ , and the corresponding  $\text{IC}_{50}$  values, obtained from the application of our molecular simulation procedure to test compound **Shire A**. As seen in Table 2, the value calculated is in outstanding agreement with the corresponding experimental result. Taken together, all these evidences constitute a proof of the validity of the overall

**Table 2.** Free energy components, total binding energy  $\Delta G_{\text{bind}}$ , and  $\text{IC}_{50}$  values resulting from molecular dynamics simulations on HCV NS5B in complex with compounds (**9–20**)

Compound	$\Delta E_{\text{vdw}}$	$\Delta E_{\text{ele}}$	$\Delta G_{\text{PB}}$	$\Delta G_{\text{NP}}$	$-T\Delta S$	$\Delta G_{\text{bind}}$	$^{\text{a}}\text{IC}_{50,\text{calc}}$
<b>9</b>	-46.5 (0.5)	-37.9 (0.5)	71.8 (0.8)	-3.9 (0.1)	10.1	<b>-6.4</b>	<b>20.0</b>
<b>10</b>	-25.6 (0.3)	-30.3 (0.6)	43.3 (0.6)	-2.9 (0.1)	9.1	<b>-6.4</b>	<b>20.0</b>
<b>11</b>	-50.2 (0.4)	-86.0 (1.0)	114.1 (1.1)	-3.5 (0.1)	19.8	<b>-5.8</b>	<b>59.0</b>
<b>12</b>	-49.1 (0.4)	-62.3 (0.9)	96.4 (0.9)	-2.9 (0.1)	11.6	<b>-6.3</b>	<b>25.0</b>
<b>13</b>	-49.3 (0.5)	-85.1 (0.8)	118.1 (1.1)	-3.1 (0.1)	14.2	<b>-5.2</b>	<b>144.0</b>
<b>14</b>	-25.4 (0.3)	-31.5 (0.4)	45.5 (0.4)	-2.9 (0.1)	8.9	<b>-5.4</b>	<b>110.0</b>
<b>15</b>	-47.2 (0.4)	-55.8 (0.5)	88.8 (0.5)	-3.2 (0.1)	10.6	<b>-6.8</b>	<b>11.0</b>
<b>16</b>	-48.3 (0.5)	-86.3 (0.6)	118.2 (0.5)	-3.4 (0.1)	13.8	<b>-6.0</b>	<b>39.0</b>
<b>17</b>	-27.2 (0.4)	-36.0 (0.5)	47.1 (0.3)	-3.2 (0.1)	12.6	<b>-6.7</b>	<b>12.0</b>
<b>18</b>	-46.0 (0.4)	-77.9 (0.8)	110.0 (0.8)	-3.1 (0.1)	11.1	<b>-5.9</b>	<b>50.0</b>
<b>19</b>	-28.9 (0.4)	-50.6 (0.3)	66.3 (0.5)	-2.9 (0.1)	9.8	<b>-6.3</b>	<b>25.0</b>
<b>20</b>	-47.1 (0.5)	-80.2 (0.9)	109.6 (0.6)	-3.5 (0.1)	14.9	<b>-6.3</b>	<b>25.0</b>
<b>Shire A</b>	-66.8 (0.4)	-89.1 (0.6)	133.1 (0.5)	-4.4 (0.1)	19.5	<b>-7.7</b>	<b>2.3 (2.2)<sup>b</sup></b>

The values obtained for the proprietary inhibitor **Shire A** are also reported for comparison. All energy values are in kcal/mol. The calculated  $\text{IC}_{50}$  values are in  $\mu\text{M}$ . The values in parentheses represent the standard error of the mean. The values of the total free energy of binding and the corresponding estimated  $\text{IC}_{50}$  values (last two columns) have been highlighted in bold for convenience.

<sup>a</sup>  $\text{IC}_{50}$  values are calculated from Eq. 4<sup>13,14</sup> (see Section 6 for details).

<sup>b</sup> Experimental value from Ref. 7.

modeling procedure adopted, from model building to protein docking and free energy calculations. Thus, we applied the same strategy for the estimation of the affinities of our set of phenantroline derivatives to HCV NS5B, as a prediction of the enzyme–drug interaction. The remaining rows of Table 2 list the results obtained for all compounds (9–20).

From the inspection of this Table we can see that the applied computational strategy is able to yield absolute free energies of binding, and hence  $IC_{50}$  values, which are quite reasonable. Further insights into the forces involved in the binding of these compounds to HCV NS5B can be found by analyzing the contributions afforded by the single components to  $\Delta G_{bind}$ , which are also listed in Table 2. Comparing the van der Waals/nonpolar ( $\Delta E_{vdW} + \Delta G_{NP}$ ) with the electrostatic ( $\Delta E_{ele} + \Delta G_{PB}$ ) contributions, we find that the association between the 12 ligands and the RdRp is mainly driven by more favorable nonpolar interactions in the complex than in the solution, in harmony with a proposed general scheme for noncovalent association.<sup>15</sup> However, as indicated for instance by the energy components of compound (13), this driving force can be considerably weakened when the polar groups on the molecule do not find an adequate bonding pattern in the protein compared to water. The free energy penalty for this ( $\Delta E_{ele} + \Delta G_{PB}$ ) is least for compound (17) and together with its substantial van der Waals contribution and moderate entropic unfavorable term consequently leads to one of the highest binding affinities in this set of phenantroline inhibitors.

Finally, we can observe a good agreement between the trend exhibited by the  $IC_{50}$  values reported in Table 2 and the corresponding biological activity determined for these compounds in BVDV infected cell lines (see Table 1). Although we obviously cannot directly compare the computed binding free energy (and hence the corresponding  $IC_{50}$ ) with the  $EC_{50}$  values derived from experiment, we can observe that, in most cases, the rank of the inhibitors with respect to their activity toward their putative targets, the RdRps of BVDV and HCV, respectively, is maintained, although with some discrepancies. This is quite reasonable if we consider that the thumb domain of the RdRps where the allosteric binding site is located is one of the most diverse features among the polymerase structures. Although there is some structural similarity between the HCV and BVDV thumb domains, the overall topology is rather different. Further, only a few of the amino acids making up the allosteric binding site are conserved in the two viral enzymes, as we inferred from our alignment of the two RdRp primary sequences (data not shown). Notwithstanding, it is important to remark here that, according to our modeling considerations reported above, the main interactions between inhibitors (9–20) and the RdRp of HCV take place with residues R422 and L474, which are conserved in the BVDV counterpart (R560 and L601, respectively); further, other interactions involve main-chain groups which do not depend on the corresponding residue side chain type. This undoubtedly contributes to justify the agreement between the different data sets.

## 5. Conclusions

In the light of the above-mentioned results, we conclude that [4,7]phenantroline derivatives showed, in general, to be endowed with good activity against viruses containing a single-stranded positive-sense RNA genome (ssRNA<sup>+</sup>) whereas 1-oxo-1,4-dihydro-[4,7]phenantrolines are less active or completely inactive. In particular in cell-based assays the compounds 9, 16, and 17 the most potent against Polio-1, CVB-2, and BVDV, respectively. Furthermore, owing to their good ratio of activity/cytotoxicity they might represent new interesting leads. Molecular modeling of the interactions between this sets of compounds and their putative final target, the HCV NS5B, confirmed both the trend in the activity of these compound and, in particular, the choice of compound (17) as a promising lead, worthy of further development as a nonnucleoside inhibitor of HCV RdRp.

In conclusion, we can affirm that [4,7]phenantrolines, owing to both the new synthetic pathway proposed and the good antiviral activities recorded, can be further developed through the introduction of alternative substituents on the position 1 and submitted to in vivo experiments.

## 6. Experimental

### 6.1. Chemistry

Melting points (mp) are uncorrected and were taken in open capillaries in a Digital Electrothermal IA9100 melting point apparatus. <sup>1</sup>H NMR spectra were recorded on a Varian XL-200 (200 MHz) instrument, using TMS as internal standard. The chemical shift values are reported in ppm ( $\delta$ ) and coupling constants ( $J$ ) in Hertz (Hz). Signal multiplicities are represented by: s (singlet), d (doublet), dd (double doublet), t (triplet), q (quadruplet) and m (multiplet). MS spectra were recorded on a combined HP 5790 (GC)-HP 5970 (MS) apparatus. Column chromatography was performed using 70–230 mesh (Merck silica gel 60). Light petroleum refers to the fraction with bp 40–60 °C. The progress of the reactions and the purity of the final compounds were monitored by TLC using Merck F-254 commercial plates. Analyses indicated by the symbols of the elements were within  $\pm 0.4\%$  of the theoretical values.

**6.1.1. Preparation of the intermediates 6-amino-7,8-dichloroquinoline (7) and diethyl 2-[(7,8-dichloroquinolin-6-ylamino)-methylene]-malonate (8).** A suspension of 2,3-dichloroaniline (1) (50.0 g, 308.6 mmol) in acetic anhydride (150 mL) was stirred at room temperature overnight, the resulting precipitate was filtered off, washed with water, and dried to afford 61.71 g (98%) of the desired 2,3-dichloroacetanilide (2). To a solution of 20 g (98.01 mmol) of anilide (2) in 100 mL of concentrated sulfuric acid, cooled at 2–5 °C, a solution of potassium nitrate (9.90 g, 9.79 mol) in 20 mL of concentrated sulfuric acid was slowly added under vigorous stirring. After the addition was complete, the reaction

mixture was stirred always below 5 °C for an additional 4 h and poured into 500 g of crushed ice. The resulting precipitate (mixture **3a** and **3b**) was filtered off and added under stirring with 150 mL of concentrated sulfuric acid. The solution obtained was heated at 100–110 °C and the stirring was continued for an additional 2 h. On cooling at room temperature, the reaction mixture was added to 600 g of crushed ice and the crude precipitate was collected by filtration and purified by chromatography on silica gel eluting with a 8:2 mixture of diethyl ether–light petroleum to yield in sequence 2,3-dichloro-6-nitroaniline (**5**) (4.87 g, 24%) and 2,3-dichloro-4-nitroaniline (**4**) (11.16 g, 55%). Six grams (28.97 mmol) of the latter compound was added to 10 g (108.87 mmol) of glycerol and 15 g (54.1 mmol) of arsenic pentoxide hydrate; the resulting mixture was then cooled to 0 °C and slowly added with 8 mL of concentrated sulfuric acid under vigorous mechanical stirring. After complete addition, the temperature was slowly raised to 150 °C and the stirring continued for an additional 3 h. On cooling at room temperature, the reaction mixture was added to 250 g of crushed ice and the crude precipitate was collected by filtration and purified by chromatography on silica gel eluting with a 8:2 mixture of diethyl ether–light petroleum to yield 4.23 g (17.40 mmol, 58%) of 7,8-dichloro-6-nitroquinoline (**6**). A solution of **6** (3.0 g, 12.4 mmol) and methyl hydrazine (3 mL) in 120 mL of ethanol was heated in a sealed steel vessel at 100 °C for 65 h. The reaction mixture was then cooled at room temperature and the solvent was removed in vacuo. The crude solid was purified by chromatography on silica gel eluting with diethyl ether to give 6-amino-7,8-dichloroquinoline (**7**) (1.58 g, 60%). Melting points, analytical, and spectroscopical data of intermediates (**2–7**) have been previously reported<sup>10</sup>. To a stirring suspension of the amine (**7**) (2.51 g, 11.8 mmol) in 40 g of Dowtherm, 3.30 g (15 mmol) of EMME was added, then the temperature was raised to 150 °C and the stirring continued for an additional 15 h. On cooling, the solution was taken up with 150 mL of hexane. The precipitate formed was filtered off and washed with hexane to give:

**6.1.1.1. Diethyl 2-[(7,8-dichloroquinol-6-ylamino)methylene]malonate (**8**).** Yield 78%, mp 171–173 °C (acetone), IR (Nujol):  $\nu_{\max}$  3158, 1697, 1655, 1589  $\text{cm}^{-1}$ ; UV (EtOH):  $\lambda_{\max}$  211, 241, 295, 329, 351 nm; <sup>1</sup>H NMR (CDCl<sub>3</sub>):  $\delta$  11.53 (d, 1H,  $J = 12.8$  Hz, NH), 8.98 (dd, 1H,  $J = 4.4$  and 1.6 Hz, H-2), 8.61 (d, 1H,  $J = 12.8$  Hz, CH=), 8.16 (dd, 1H,  $J = 8.2$  e 1.6 Hz, H-4), 7.57 (s, 1H, H-5), 7.51 (dd, 1H,  $J = 8.2$  e 4.4 Hz, H-3), 4.36 (m, 4H, 2 CH<sub>2</sub>), 1.39 (m, 6H, 2 CH<sub>3</sub>); MS  $m/z$  382/384/386 (M<sup>+</sup>). Anal. C<sub>17</sub>H<sub>16</sub>Cl<sub>2</sub>N<sub>4</sub>O<sub>4</sub> (C, H, N).

**6.1.2. Preparation of 5,6-dichloro-[4,7]phenantroline (**9**).** To a mixture of **7** (3.0 g, 14.1 mmol), glycerol (5.4 g, 58 mmol), and arsenic pentoxide hydrate (10.0 g, 31 mmol), cooled at 0 °C, 4 mL of concentrated sulfuric acid was slowly added under vigorous mechanical stirring. After addition, the temperature was slowly raised to 150 °C and the stirring continued for an additional 2 h. The mixture was then cooled to room temperature, poured into 250 g of crushed ice, and the crude precipi-

tate was collected by filtration and crystallized by ethanol to yield 3.06 g (86% of yield) of **9**. Mp 265–266 °C, IR (Nujol):  $\nu_{\max}$  1650, 1570  $\text{cm}^{-1}$ ; UV (EtOH):  $\lambda_{\max}$  224, 258, 289, 373 nm; <sup>1</sup>H NMR (CDCl<sub>3</sub>+DMSO-*d*<sub>6</sub>):  $\delta$  9.15 (dd, 2H,  $J = 4.6$  and 1.6 Hz, H-3 + H-8), 9.08 (d, 2H,  $J = 8.4$  Hz, H-1 + H-10), 7.78 (dd, 2H,  $J = 4.6$  and 1.6 Hz, H-2 + H-9); MS  $m/z$  248/250/252 (M<sup>+</sup>). Anal. C<sub>12</sub>H<sub>6</sub>Cl<sub>2</sub>N<sub>2</sub> (C, H, N).

**6.1.3. Preparation of [4,7]phenantroline (**10**).** A suspension of **9** (1.0 g, 4 mmol), 10% palladium–charcoal (0.20 g), and 3 mL of hydrazine monohydrate (98%) in 20 mL of ethanol was refluxed under stirring for 2.5 h. On cooling, the catalyst was filtered off and the solvent and the excess of hydrazine were removed in vacuo. The crude solid was recrystallized by acetone to yield 0.38 g (54% yield) of **10**. Mp 217–218 °C, IR (Nujol):  $\nu_{\max}$  1623, 1597  $\text{cm}^{-1}$ ; UV (EtOH):  $\lambda_{\max}$  232, 274 nm; <sup>1</sup>H NMR (DMSO-*d*<sub>6</sub>):  $\delta$  9.71 (d, 2H,  $J = 5.4$  Hz, H-3 + H-8), 9.26 (d, 2H,  $J = 8.6$  Hz, H-1 + H-10), 8.53 (s, 2H, H-5 + H-6), 8.10 (d, 2H,  $J = 8.6$  and 5.4 Hz, H-2 + H-9); MS  $M/Z$  180 (M<sup>+</sup>). Anal. C<sub>12</sub>H<sub>8</sub>N<sub>2</sub> (C, H, N).

**6.1.4. Preparation of 5,6-dichloro-1-oxo-1,4-dihydro-[4,7]phenantroline-2-carboxylic acid ethyl ester (**11**) and 5,6-dichloro-1-oxo-1,4-dihydro-[4,7]phenantroline (**12**).** Intermediate (**8**) (3.0 g, 7.8 mmol) was suspended in 50 g of Dowtherm and heated at 250 °C under stirring for 2.5 h. On cooling, it was taken up with 200 mL of hexane. The precipitate formed was filtered off and chromatographed on silica gel eluting with a 9:1 mixture of diethyl ether–light petroleum to yield in sequence **11** (1.34 g, 51%) and **12** (0.40 g, 20%). Continuing the stirring at 250 °C for an additional 12.5 h, after dilution of the Dowtherm solution, gave the sole compound (**12**) in 69% yield. Alternatively, by submitting the ester (**11**) (1.0 g, 3.0 mmol) to the same reaction in 20 g of Dowtherm at 250 °C under stirring for 13 h, compound (**12**) was obtained in 81% yield.

**6.1.4.1. 5,6-Dichloro-1-oxo-1,4-dihydro-[4,7]phenantroline-2-carboxylic acid ethyl ester (**11**).** Mp 235–237 °C (acetone), IR (Nujol):  $\nu_{\max}$  3196, 1714, 1615  $\text{cm}^{-1}$ ; UV (EtOH):  $\lambda_{\max}$  211, 225, 253, 281, 342, 358 nm; <sup>1</sup>H NMR (DMSO-*d*<sub>6</sub>):  $\delta$  12.16 (s, 1H, NH), 10.47 (d, 1H,  $J = 8.8$  Hz, H-8), 9.01 (dd, 1H,  $J = 4.2$  Hz, H-10), 8.39 (s, 1H, H-3), 7.79 (dd, 1H,  $J = 8.8$  and 4.2 Hz, H-9), 4.28 (q, 2H,  $J = 7.0$  Hz, CH<sub>2</sub>), 1.33 (t, 3H,  $J = 7.0$  Hz, CH<sub>3</sub>); MS  $m/z$  336/338/340 (M<sup>+</sup>). Anal. C<sub>15</sub>H<sub>10</sub>Cl<sub>2</sub>N<sub>2</sub>O<sub>3</sub> (C, H, N).

**6.1.4.2. 5,6-Dichloro-1-oxo-1,4-dihydro-[4,7]phenantroline (**12**).** Mp > 300 °C (ethanol), IR (Nujol):  $\nu_{\max}$  3467, 3389, 1624  $\text{cm}^{-1}$ ; UV (EtOH):  $\lambda_{\max}$  226, 272, 344, 358 nm; <sup>1</sup>H NMR (DMSO-*d*<sub>6</sub>):  $\delta$  11.85 (s, 1H, NH), 10.66 (d, 1H,  $J = 8.8$  Hz, H-8), 9.00 (d, 1H,  $J = 4.2$  Hz, H-10), 7.94 (d, 1H,  $J = 7.2$  Hz, H-3), 7.80 (dd, 1H,  $J = 8.8$  and 4.2 Hz, H-9), 6.43 (d, 1H,  $J = 7.2$  Hz, H-2); MS  $m/z$  250/252/254 (M<sup>+</sup>). Anal. C<sub>12</sub>H<sub>6</sub>Cl<sub>2</sub>N<sub>2</sub>O (C, H, N).

**6.1.5. Preparation of 5,6-dichloro-1-oxo-1,4-dihydro-[4,7]phenantroline-2-carboxylic acid (**13**).** The ester (**11**) (0.5 g, 1.4 mmol) was dissolved in 50 mL of concentrated

sulfuric acid and heated at 100–110 °C under stirring for 2 h. On cooling, the solution was poured onto 50 g of crushed ice. The crude precipitate formed was collected by filtration and crystallized by ethanol to yield 0.41 g (91% of yield) of **13**. Mp > 300 °C, IR (Nujol):  $\nu_{\max}$  3558, 3401, 1715, 1617  $\text{cm}^{-1}$ ; UV (EtOH):  $\lambda_{\max}$  207, 252, 279, 338, 354 nm;  $^1\text{H}$  NMR (DMSO- $d_6$ ):  $\delta$  10.29 (d, 1H,  $J$  = 8.8 Hz, H-8), 9.03 (d, 1H,  $J$  = 4.2 Hz, H-10), 8.69 (d, 1H,  $J$  = 7.2 Hz, H-3), 7.82 (dd, 1H,  $J$  = 8.8 and 4.2 Hz, H-9); MS  $m/z$  308/310/312 ( $\text{M}^+$ ). Anal.  $\text{C}_{13}\text{H}_6\text{Cl}_2\text{N}_2\text{O}_3$  (C, H, N).

**6.1.6. Preparation of 1-oxo-1,4-dihydro-[4,7]phenantrolin-14**. A suspension of **12** (0.6 g, 1.2 mmol), 10% palladium–charcoal (0.12 g), and 1 mL of hydrazine monohydrate (98%) in 15 mL of ethanol was refluxed under stirring for 2.5 h. The reaction mixture was then cooled at room temperature, the catalyst was filtered off, and the solvent and the excess of hydrazine were removed in vacuo. The crude solid was recrystallized by acetone to yield 0.26 g (56% yield) of **14**. Mp 280–281 °C, IR (Nujol):  $\nu_{\max}$  3472, 3403, 1638, 1605  $\text{cm}^{-1}$ ; UV (EtOH):  $\lambda_{\max}$  221, 263, 327, 336, 349 nm;  $^1\text{H}$  NMR (DMSO- $d_6$ ):  $\delta$  11.47 (s, 1H, NH), 10.84 (d, 1H,  $J$  = 8.0 Hz, H-8), 9.16 (d, 1H,  $J$  = 4.2 Hz, H-10), 8.51 (d, 1H, 9.2 Hz, H-6), 8.37–8.26 (m, 2H, H-3 + H-5), 8.08 (dd, 1H,  $J$  = 8.0 and 4.2 Hz, H-9), 6.72 (d, 1H,  $J$  = 7.0 Hz, H-2); MS  $m/z$  196 ( $\text{M}^+$ ). Anal.  $\text{C}_{12}\text{H}_8\text{N}_2\text{O}$  (C, H, N).

**6.1.7. Preparation of 5,6-dichloro-1-ethoxy-[4,7]phenantrolin-16**. A suspension of **12** (1.0 g, 4 mmol) and 1.30 g (4 mmol) of cesium carbonate (99%) in 20 mL of dehydrated dimethylformamide (less than 0.0100% of water) (DMF) was heated under stirring at 60 °C and slowly added with a solution of ethyl sulfate (0.74 g, 4.8 mmol) in 6 mL DMF. After the addition was complete, the reaction mixture was stirred for an additional 4 h and poured into 200 g of crushed ice. The solid obtained was recrystallized by diethyl ether to yield 0.84 g (72% yield) of **16**. Mp 201–203 °C, IR (Nujol):  $\nu_{\max}$  1674, 1580  $\text{cm}^{-1}$ ; UV (EtOH):  $\lambda_{\max}$  213, 240, 312, 328 nm;  $^1\text{H}$  NMR (DMSO- $d_6$ ):  $\delta$  9.46 (d, 1H,  $J$  = 8.4 Hz, H-8), 8.89 (d, 1H,  $J$  = 4.4 Hz, H-10), 8.73 (d, 1H,  $J$  = 8.0 Hz, H-3), 7.63 (dd, 1H,  $J$  = 8.8 and 4.4 Hz, H-9), 7.23 (d, 1H,  $J$  = 8.0 Hz, H-2), 4.30 (q, 2H,  $J$  = 7.0 Hz,  $\text{CH}_2$ ), 1.33 (t, 3H,  $J$  = 7.0 Hz,  $\text{CH}_3$ ); MS  $m/z$  292/294/296 ( $\text{M}^+$ ). Anal.  $\text{C}_{14}\text{H}_{10}\text{Cl}_2\text{N}_2\text{O}$  (C, H, N).

**6.1.8. Preparation of 1-ethoxy-[4,7]phenantrolin-17**. A suspension of **16** (0.6 g, 2.4 mmol), 10% palladium–charcoal (0.12 g), and 2 mL of hydrazine monohydrate (98%) in 15 mL of ethanol was refluxed under stirring for 2.5 h. On cooling, the catalyst was filtered off and the solvent and the excess of hydrazine were removed in vacuo. The crude solid was recrystallized by acetone to yield 0.24 g (52% yield) of **17**. Mp 172–173 °C, IR (Nujol):  $\nu_{\max}$  1662, 1580  $\text{cm}^{-1}$ ; UV (EtOH):  $\lambda_{\max}$  208, 246, 263, 338 nm;  $^1\text{H}$  NMR (DMSO- $d_6$ ):  $\delta$  9.42 (d, 1H,  $J$  = 8.4 Hz, H-8), 8.92 (d, 1H,  $J$  = 4.4 Hz, H-10), 8.78 (d, 1H,  $J$  = 8.0 Hz, H-3), 8.36 (d, 1H,  $J$  = 9.2 Hz, H-6), 8.25 (d, 1H,  $J$  = 9.2 Hz, H-5), 7.88 (dd, 1H,  $J$  = 8.4 and 4.4 Hz, H-9), 7.59 (d, 1H,  $J$  = 8.0 Hz,

H-2), 4.46 (q, 2H,  $J$  = 7.0 Hz,  $\text{CH}_2$ ), 1.38 (t, 3H,  $J$  = 7.0 Hz,  $\text{CH}_3$ ); MS  $m/z$  224 ( $\text{M}^+$ ). Anal.  $\text{C}_{14}\text{H}_{12}\text{N}_2\text{O}$  (C, H, N).

**6.1.9. Preparation of 1,5,6-trichloro-[4,7]phenantrolin-15**. A solution of **12** (1.50 g, 6 mmol) in 20 mL of phosphorus(V)oxychloride (99%) was refluxed under stirring for 48 h. The reaction mixture was then cooled at room temperature and poured into 200 g of crushed ice and the resulting solution was made alkaline with 25% ammonia solution. The crude solid obtained was purified by chromatography on silica gel with a 9:1 mixture of chloroform–methanol to give **15** (1.2 g, 72%). Mp 238–240 °C (ethanol), IR (Nujol):  $\nu_{\max}$  1586, 1564  $\text{cm}^{-1}$ ; UV (EtOH):  $\lambda_{\max}$  211, 238, 271 nm;  $^1\text{H}$  NMR (DMSO- $d_6$ ):  $\delta$  10.07 (d, 1H,  $J$  = 8.4 Hz, H-8), 9.13 (d, 1H,  $J$  = 4.2 Hz, H-10), 8.98 (d, 1H,  $J$  = 8.4 Hz, H-3), 8.03 (d, 1H,  $J$  = 8.4 Hz, H-2), 7.88 (dd, 1H,  $J$  = 8.8 and 4.2 Hz, H-9); MS  $m/z$  282/284/286 ( $\text{M}^+$ ). Anal.  $\text{C}_{12}\text{H}_5\text{Cl}_2\text{N}_2$  (C, H, N).

**6.1.10. Preparation of 1-amine-5,6-dichloro-[4,7]phenantrolin-18**. A solution of **15** (2.44 g, 7.72 mmol) in 250 mL of ethanol saturated with dry gaseous ammonia was heated in a sealed steel vessel at 160 °C under stirring for 72 h. Then the reaction mixture was cooled at room temperature, the solvent was removed in vacuo, and the solid residue chromatographed on silica gel with a 9:1 mixture of chloroform–methanol to give in sequence **18** (1.94 g, 85%) and 0.14 g (5%) of **16**. Mp 261–263 °C (ethanol), IR (Nujol):  $\nu$  3450, 3311, 1636, 1583  $\text{cm}^{-1}$ ; UV (EtOH):  $\lambda_{\max}$  210, 232, 280, 358 nm;  $^1\text{H}$  NMR (DMSO- $d_6$ ):  $\delta$  9.42 (d, 1H,  $J$  = 8.6 Hz, H-8), 8.99 (d, 1H,  $J$  = 4.2 Hz, H-10), 8.49 (d, 1H,  $J$  = 8.4 Hz, H-3), 7.77 (dd, 1H,  $J$  = 8.6 and 4.2 Hz, H-9), 7.09 (d, 1H,  $J$  = 8 Hz, H-2), 7.04 (s, 2H,  $\text{NH}_2$ ); MS  $m/z$  263/265/267 ( $\text{M}^+$ ). Anal.  $\text{C}_{12}\text{H}_7\text{Cl}_2\text{N}_3$  (C, H, N).

**6.1.11. Preparation of 1-amine-[4,7]phenantrolin-19**. A suspension of **18** (0.48 g, 1.82 mmol), 10% palladium–charcoal (0.10 g), and 2 mL of hydrazine monohydrate (98%) in 15 mL of ethanol was refluxed under stirring for 2.5 h. On cooling, the catalyst was filtered off and the solvent and the excess of hydrazine were removed in vacuo. The crude solid was recrystallized by acetone to yield 0.34 g (94% yield) of **19**. Mp 288–290 °C, IR (Nujol):  $\nu_{\max}$  3267, 3096, 1661, 1630, 1608  $\text{cm}^{-1}$ ; UV (EtOH):  $\lambda_{\max}$  234, 265, 333, 349 nm;  $^1\text{H}$  NMR (DMSO- $d_6$ ):  $\delta$  9.26 (d, 1H,  $J$  = 8.6 Hz, H-8), 9.14 (s, 2H,  $\text{NH}_2$ ), 9.06 (d, 1H,  $J$  = 4.4 Hz, H-10), 8.48 (d, 1H,  $J$  = 7.0 Hz, H-3), 8.39 (d, 1H,  $J$  = 9.2 Hz, H-6), 8.32 (d, 1H,  $J$  = 9.2 Hz, H-5), 7.82 (dd, 1H,  $J$  = 8.6 and 4.4 Hz, H-9), 7.28 (d, 1H,  $J$  = 7.0 Hz, H-2); MS  $m/z$  195 ( $\text{M}^+$ ). Anal.  $\text{C}_{12}\text{H}_9\text{N}_3$  (C, H, N).

**6.1.12. Preparation of N-(5,6-dichloro-[4,7]phenantrolin-1-yl)-acetamide (20)**. A suspension of **18** (0.24 g, 0.91 mmol) in 10 mL of acetic anhydride was stirred at rt for 24 h and the crude precipitate was collected by filtration and recrystallized by ethanol to yield **20** (0.22 g, 78%). Mp 254 °C (dec), IR (Nujol):  $\nu$  3312, 1662,

1613  $\text{cm}^{-1}$ ; UV (EtOH):  $\lambda_{\text{max}}$  213, 231, 281, 324, 360 nm;  $^1\text{H}$  NMR (DMSO- $d_6$ ):  $\delta$  12.11 (s, 1H, NH), 9.42 (d, 1H,  $J = 8.0$  Hz, H-8), 8.99 (d, 1H,  $J = 4.2$  Hz, H-10), 8.48 (d, 1H,  $J = 8.4$  Hz, H-3), 7.76 (dd, 1H,  $J = 8.0$  and 4.2 Hz, H-9), 7.15 (d, 1H,  $J = 8$  Hz, H-2), 1.93 (s, 3H,  $\text{CH}_3$ ); MS  $m/z$  305/307/309 ( $\text{M}^+$ ). Anal.  $\text{C}_{14}\text{H}_9\text{Cl}_2\text{N}_3\text{O}$  (C, H, N).

## 6.2. Cell-based assays

**6.2.1. Compounds.** Compounds were dissolved in 100 mM DMSO and then diluted in culture medium.

**6.2.2. Cells and viruses.** Cell lines were purchased from American Type Culture Collection (ATCC). The absence of mycoplasma contamination was checked periodically by the Hoechst staining method. Cell lines supporting the multiplication of RNA viruses were as follows: Madin Darby Bovine Kidney (MDBK); Baby Hamster Kidney (BHK-21);  $\text{CD4}^+$  human T-cells containing an integrated HTLV-1 genome (MT-4); Monkey kidney (Vero 76) cells.

**6.2.3. Cytotoxicity assays.** For cytotoxicity tests, run in parallel with antiviral assays, MDBK, BHK, and Vero 76 cells were resuspended in 96-multiwell plates at an initial density of  $6 \times 10^5$ ,  $1 \times 10^6$ , and  $5 \times 10^5$  cells/mL, respectively, in maintenance medium, without or with serial dilutions of test compounds. Cell viability was determined after 48–120 h at 37 °C in a humidified  $\text{CO}_2$  (5%) atmosphere by the MTT method. The cell number of Vero 76 monolayers was determined by staining with the crystal violet dye.

For cytotoxicity evaluations, exponentially growing cells derived from human hematological tumors [ $\text{CD4}^+$  human T-cells containing an integrated HTLV-1 genome (MT-4)] were seeded at an initial density of  $1 \times 10^5$  cells/mL in 96-well plates in RPMI-1640 medium supplemented with 10% fetal calf serum (FCS), 100 U/mL penicillin G, and 100  $\mu\text{g}/\text{mL}$  streptomycin. Cell cultures were then incubated at 37 °C in a humidified, 5%  $\text{CO}_2$  atmosphere in the absence or presence of serial dilutions of test compounds. Cell viability was determined after 96 h at 37 °C by the 3-(4,5-dimethylthiazol-2-yl)-2,5-diphenyl-tetrazolium bromide (MTT) method.<sup>16</sup>

**6.2.4. Antiviral assays.** Activity of compounds against yellow fever virus (YFV) was based on inhibition of virus-induced cytopathogenicity in acutely infected BHK-21 cells.

Activity against bovine viral diarrhoea virus (BVDV), in infected MDBK cells, was based on inhibition of virus-induced cytopathogenicity.

BHK and MDBK were seeded in 96-well plates at a density of  $5 \times 10^4$  and  $3 \times 10^4$ , and  $2.5 \times 10^4$  cells/well, respectively, and were allowed to form confluent monolayers by incubating overnight in growth medium at 37 °C in a humidified  $\text{CO}_2$  (5%) atmosphere. Cell monolayers were then infected with 50  $\mu\text{L}$  of a proper virus

dilution (in serum-free medium) to give an moi, 0.01 (0.04 in the case of RSV). One hour later, 50  $\mu\text{L}$  of MEM Earle's medium (Dulbecco's modified Eagle's medium for Vero/RSV), supplemented with inactivated fetal calf serum (FCS), 1% final concentration, without or with serial dilutions of test compounds, was added. After a 2–3-day incubation at 37 °C, cell viability was determined by the MTT method. Activity of compounds against Coxsackie virus, B-2 strain (CVB-2), Polio virus type-1 (Polio-1), Sabin strain, was determined by plaque reduction assays in Vero 76 cell monolayers. To this end, Vero 76 cells were seeded in 24-well plates at a density of  $2 \times 10^5$  cells/well and were allowed to form confluent monolayers by incubating overnight in growth medium at 37 °C in a humidified  $\text{CO}_2$  (5%) atmosphere. Then, monolayers were infected with 250  $\mu\text{L}$  of proper virus dilutions to give 50–100 PFU/well. Following removal of unabsorbed virus, 500  $\mu\text{L}$  of Dulbecco's modified Eagle's medium supplemented with 1% inactivated FCS and 0.75% methyl cellulose, without or with serial dilutions of test compounds, was added. Cultures were incubated at 37 °C for 2 (Sb-1), 3 (CVB-2) days and then fixed with PBS containing 50% ethanol and 0.8% crystal violet, washed, and air-dried. Plaques were then counted. 50% effective concentrations ( $\text{EC}_{50}$ ) were calculated by linear regression technique.

## 6.3. Molecular modeling

All molecular dynamics simulations were run on a cluster of Silicon Graphics Octane RK12. The entire computational recipe involved the following program packages: AutoDock (v. 3.0),<sup>17</sup> AMBER 7.0,<sup>18,19</sup> *Materials Studio* (v.3.2, Accelrys Inc., San Diego, CA, USA), and in-house developed codes (stand-alone and add-on to the commercial software).

The starting 3-D model of the HCV RNA-dependent RNA polymerase was based on its X-ray crystallographic structure (chain B, PDB Code: 1CSJ).<sup>20</sup> Missing hydrogen atoms were added to the protein backbone and side chains with the parse module of Amber 7.0. All ionizable residues were considered in the standard ionization state at neutral pH. The geometry of added hydrogen was refined for 200 steps (steepest descent) in vacuum, using the well-validated, all-atom force field (FF) parameter set (*parm94*) by Cornell et al.<sup>21</sup> Further protein geometry refinement was carried out using the *Sander* module of Amber 7.0 via a combined steepest descent—conjugate gradient algorithm, using as a convergence criterion for the energy gradient the root-mean-square of the Cartesian elements of the gradient equal to 0.01 kcal/(mol Å). The generalized Born/surface area (GB/SA) continuum solvation model.<sup>22,23</sup> was used to mimic a water environment.<sup>22,23</sup> As expected, no relevant structural changes were observed between RdRp relaxed model and the original 3-D structure.

The model structures of all title compounds were built and subjected to an initial energy minimization, again using the *Sander* module of the Amber 7.0 suite of programs, with the *parm94* version of the Amber force field. In this case, the convergence criterion was set to

$10^{-4}$  kcal/(mol Å). A conformational search was carried out using a well-validated, ad hoc developed combined molecular mechanics/molecular dynamics simulated annealing (MDSA) protocol.<sup>24–28</sup> Accordingly, the relaxed structures were subjected to five repeated temperature cycles (from 310 to 1000 K and back) using constant volume/constant temperature (NVT) MD conditions. At the end of each annealing cycle, the structures were again energy minimized to converge below  $10^{-4}$  kcal/(mol Å), and only the structures corresponding to the minimum energy were used for further modeling. The atomic partial charges for the geometrically optimized compounds were obtained using the RESP procedure,<sup>29</sup> and the electrostatic potentials were produced by single-point quantum mechanical calculations at the Hartree–Fock level with a 6-31G\* basis set, using the Merz–Singh–Kollman van der Waals parameters.<sup>30,31</sup> Eventual missing force field parameters for the phenantrolin derivatives were generated as follows: AM1<sup>32</sup> geometry optimization of the structure was followed by RHF/6-31G\* single point calculation to obtain the electrostatic potentials. Next, the RESP method was used for charge fitting. The missing bond, torsion angle or van der Waals parameters not included in the *parm94* were transferred<sup>33</sup> from the newly developed *parm99* parameter set.<sup>34</sup>

The optimized structures of the test compounds were docked into the HCV polymerase allosteric binding site by applying a consolidated procedure;<sup>25,26,28</sup> accordingly, it will be described here only briefly. The software AutoDock 3.0<sup>17</sup> was employed to estimate the possible binding orientations of all compounds in the receptor. In order to encase a reasonable region of the protein surface and interior volume, centered on the crystallographically identified binding site, the grids were 60 Å on each side. Grid spacing (0.375 Å) and 120 grid points were applied in each Cartesian direction so as to calculate mass-centered grid maps. Amber 12–6 and 12–10 Lennard–Jones parameters were used in modeling van der Waals interactions and hydrogen bonding (N–H, O–H, and S–H), respectively. In the generation of the electrostatic grid maps, the distance-dependent relative permittivity of Mehler and Solmajer was applied.<sup>35</sup> For the docking of each compound to the protein, three hundred Monte Carlo/Simulated Annealing (MC/SA) runs were performed, with 100 constant temperature cycles for simulated annealing. For these calculations, the GB/SA implicit water model<sup>22,23</sup> was again used to mimic the solvated environment. The rotation of the angles  $\phi$  and  $\varphi$ , and the angles of side chains were set free during the calculations. All other parameters of the MC/SA algorithm were kept as default. Following the docking procedure, the structures of all compounds were subjected to cluster analysis with a tolerance of 1 Å for an all-atom root-mean-square (RMS) deviation from a lower-energy structure representing each cluster family. In the absence of any relevant crystallographic information, the structure of each resulting complex characterized by the lowest interaction energy in the prevailing cluster was selected for further evaluation.

Each best substrate/RdRp complex resulting from the automated docking procedure was further refined in

the Amber 7.0 suite using the quenched molecular dynamics (QMD) method.<sup>36</sup> In this case, 100 ps MD simulation at 310 K were employed to sample the conformational space of the substrate–enzyme complex in the GB/SA continuum solvation environment.<sup>22,23</sup> The integration step was equal to 1 fs. After each ps, the system was cooled to 0 K, the structure was extensively minimized, and stored. To prevent global conformational changes of the enzyme, the backbone of the protein binding site was constrained by a harmonic force constant of 100 kcal/Å, whereas the amino acid side chains and the ligands were allowed to move without any constraint.

The best energy configuration of each complex resulting from the previous step was allowed to relax in a 55-Å radius sphere of TIP3P water molecules.<sup>37</sup> The resulting system was minimized with a gradual decrease in the position restraints of the protein atoms. At the end of the relaxation process, all water molecules beyond the first hydration shell (i.e., at a distance of  $>3.5$  Å from any protein atom) were removed. Finally, to achieve electro-neutrality, a suitable number of counterions were added, in the positions of largest electrostatic potential, as determined by the module *Cion* within Amber 7.0. To reduce computational time to reasonable limits, all protein residues with any atom closer than 20 Å from the center of mass of each bound ligand were chosen to be flexible in the dynamic simulations. Subsequently, a spherical TIP3P water cap of radius equal to 20 Å was centered on each inhibitor in the corresponding RdRp complex, including the hydrating water molecules within the sphere resulting from the previous step. After energy minimization of the new water cap for 1500 steps, keeping the protein, the ligand, and the pre-existing waters rigid, followed by a MD equilibration of the entire water sphere with fixed solute for 20 ps, further unfavorable interactions within the structures were relieved by progressively smaller positional restraints on the solute (from 25 to 0 kcal/(mol Å<sup>2</sup>) for a total of 4000 steps. Each system was gradually heated to 310 K in three intervals, allowing a 5-ps interval per 100 K, and then equilibrated for 50-ps at 310 K, followed by 400-ps of data collection runs, necessary for the estimation of the free energy of binding (vide infra). The MD simulations were performed at constant  $T = 310$  K using the Berendsen et al. coupling algorithm<sup>38</sup> with separate coupling of the solute and solvent to the heat, an integration time step of 2-fs, and the applications of the *Shake* algorithm<sup>39</sup> to constrain all bonds to their equilibrium values, thus removing high frequency vibrations. Long-range nonbonded van der Waals interactions were truncated by using a dual cutoff of 9 and 13 Å, respectively, where energies and forces due to interactions between 9 and 13 Å were updated every 20-time steps. The particle mesh Ewald method<sup>40</sup> was used to treat the long-range electrostatics. For the calculation of the binding free energy between the RdRp and each phenantrolin derivative in water, a total of 400 snapshots were saved during the MD data collection period described above, one snapshot per 1 ps of MD simulation.

The binding free energy  $\Delta G_{\text{bind}}$  of each RdRp/drug complex in water was calculated according to the procedure

termed Molecular Mechanic/Poisson–Boltzmann Surface Area (MM/PBSA), and originally proposed by Srinivasan et al.<sup>41</sup> Since the theoretical background of this methodology is described in details in the original papers by Peter Kollman and his group,<sup>42</sup> it will be only briefly described below.

Basically, an MD simulation (typically in explicit solvent) is first carried out which yields a representative ensemble of structures. The average total free energy of the system,  $G$ , is then evaluated as:

$$G = G_{\text{PB}} + G_{\text{NP}} + E_{\text{MM}} - TS_{\text{solute}} \quad (1)$$

in which  $G_{\text{PB}}$  is the polar solvation energy component, which is calculated in a continuum solvent, usually a finite-difference Poisson–Boltzmann (PB) model, and  $G_{\text{NP}}$  is the nonpolar contribution to the solvation energy, which can be obtained from the solvent accessible surface area (SA).  $E_{\text{MM}}$  denotes the sum of molecular mechanics (MM) energies of the molecule, and can be further split into contributions from electrostatic ( $E_{\text{ele}}$ ) and van der Waals ( $E_{\text{vdw}}$ ) energies:

$$E_{\text{MM}} = E_{\text{ele}} + E_{\text{vdw}} \quad (2)$$

The last term in Eq. 1,  $TS_{\text{solute}}$  represents the solute entropy, and is usually estimated by a combination of classical statistical formulas and normal mode analysis.

The binding free energy  $\Delta G_{\text{bind}}$  of a given noncovalent association can then be obtained as:

$$\begin{aligned} \Delta G_{\text{bind}} &= G_{\text{complex}} - (G_{\text{protein}} + G_{\text{ligand}}) \\ &= \Delta E_{\text{MM}} + \Delta G_{\text{solv}} - T\Delta S \end{aligned} \quad (3)$$

in which  $\Delta G_{\text{solv}} = \Delta G_{\text{PB}} + \Delta G_{\text{NP}}$ . The ensemble of structures for the uncomplexed reactants are generated either running separate MD simulations for them, or by using the trajectory of the complex, simply removing the atoms of the protein or ligand. As reported below, in this work we followed the successful approach proposed by Kuhn and Kollman<sup>43</sup> and applied the latter variant. Accordingly, the  $E_{\text{MM}}$  were calculated with the *Anal* and *Carnal* modules from the AMBER 7.0 suite. The infinite cutoffs for all interactions and the *parm94* force field parameters were applied.<sup>21</sup> The calculations of the polar solvation term  $G_{\text{PB}}$  were done with the *Delphi* package,<sup>44</sup> with interior and exterior dielectric constants equal to 1 and 80, respectively. A grid spacing of 2/Å, extending 20% beyond the dimensions of the solute, was employed. The nonpolar component  $G_{\text{NP}}$  was obtained using the following relationship:<sup>45</sup>  $G_{\text{NP}} = \gamma SA + b$ , in which  $\gamma = 0.00542$  kcal/(mol Å<sup>2</sup>),  $b = 0.92$  kcal/mol, and the surface area was estimated by means of the MSMS software.<sup>46</sup> The last parameter in Eq. 1, i.e., the change in solute entropy upon association— $TS_{\text{solute}}$ , was calculated through normal-mode analysis.<sup>47</sup> In the first step of this calculation, an 8-Å sphere around the ligand was cut out from an MD snapshot for each ligand–protein complex. This value was shown to be large enough to yield converged mean changes in solute entropy. On the basis of the size-reduced snapshots, of the complex, we generated structures of the uncomplexed reactants by removing the atoms of the protein and ligand, respec-

tively. Each of those structures was minimized, using a distance-dependent dielectric constant  $\epsilon = 4r$ , to account for solvent screening, and its entropy was calculated using classical statistical formulas and normal mode-analysis. To minimize the effects due to different conformations adopted by individual snapshots we averaged the estimation of entropy over 10 snapshots.

Finally, the  $IC_{50}$  values were calculated from the corresponding binding free energies using the following relationship:<sup>13,14</sup>

$$\begin{aligned} \Delta G_{\text{bind}} &= RT \ln K_{\text{diss}} = RT \ln (IC_{50} + 0.50C_{\text{enz}}) \\ &\cong RT \ln IC_{50} \end{aligned} \quad (4)$$

The overall quality of the entire procedure described above, i.e., protein and inhibitors modeling, conformational analysis, docking, and energetic calculations—was tested by carrying out the same calculations for one proprietary inhibitor, **Shire A**, from Shire BioChem Inc., characterized by a structure reminiscent of that characterizing some of the title compounds, and for which both the crystallographic structures of the relevant HCV RdRp complexes (PBD entry codes: 1NHU) and the corresponding  $IC_{50}$  values were available.<sup>7</sup>

All modeling figures were prepared using Chimera.<sup>48</sup>

## References and notes

1. Tan, S. L.; Pause, A.; Shi, Y.; Sonenberg, N. *Nat. Rev. Drug. Discov.* **2002**, *1*, 867.
2. Hayashi, P. H.; Di Bisceglie, A. M. *Med. Clin. North Am.* **2005**, *89*, 371.
3. Memon, M. I.; Memon, M. A. *J. Viral Hepat.* **2002**, *9*, 84.
4. Echevarria-Mayo, J. M. *Enferm. Infecc. Microbiol. Clin.* **2006**, *24*, 45.
5. Bosch, F. X.; Ribes, J.; Cleries, R.; Diaz, M. *Clin. Liver Dis.* **2005**, *9*, 191.
6. Enterovirus surveillance: MMWR Morb. Mortal Wkly Rep. **2006**, *55*, 153.
7. Wang, M.; Ng, K. K.-S.; Cherney, M. M.; Chan, L.; Yannopoulos, C. G.; Bedard, J.; Morin, N.; Nguyen-Ba, N.; Alaoui-Ismaili, M. H.; Bethell, R. C.; James, M. N. C. *J. Biol. Chem.* **2003**, *278*, 9489.
8. Kaufmann, A.; Radosevic, R. *Chem. Ber.* **1909**, *42*, 2613.
9. (a) Albert, A.; Brown, D. J.; Heinz, D. *J. Chem. Soc.* **1948**, 1285; (b) Douglas, B.; Kermack, W. O. *J. Chem. Soc.* **1949**, 1017; (c) Sykes, W. O. *J. Chem. Soc.* **1953**, 3543.
10. Sanna, P.; Carta, A.; Paglietti, G. *Heterocycles* **2000**, *53*, 423.
11. Carta, A.; Boatto, G.; Paglietti, G.; Poni, G.; Setzu, M. G.; Caredda, P. *Heterocycles* **2003**, *60*, 833.
12. Pricl, S.; Manfredini, S.; Angusti, A.; Ciliberti, N.; Durini, E.; Vertuani, S.; Buzzoni, L.; Coslanich, A.; Ferrone, M.; Fermiglia, M.; Paneni, M. S.; La Colla, P.; Sanna, G.; Cadeddu, A.; Mura, M.; Loddo, R. In *Framing the Knowledge of Therapeutics for Viral Hepatitis*; Schinazi, R. F., Schiff, E. R., Eds.; IHL Press: Arlington, MA, USA, 2006; p 279.
13. Kroeger Smith, M. B.; Lamb, M. L.; Tirado-Rives, J.; Jorgensen, W. L.; Michejda, C. J.; Ruby, S. K.; Smith, R. H., Jr. *Protein Eng.* **2000**, *13*, 413.
14. Wang, J.; Morin, P.; Wang, W.; Kollman, P. A. *J. Am. Chem. Soc.* **2001**, *123*, 5221.

15. Miyamoto, S.; Kollman, P. A.. *Proc. Natl. Acad. Sci. U.S.A.* **1993**, *90*, 8402.
16. Pawels, R.; Balzarini, J.; Baba, M.; Snoeck, R.; Schols, D.; Herdewijn, P.; Desmyster, J.; De Clercq, E. *J. Virol. Methods* **1998**, *20*, 309.
17. Morris, G. M.; Goodsell, D. S.; Halliday, R. S.; Huey, R.; Hart, W. E.; Belew, R. K.; Olson, A. J. *J. Comput. Chem.* **1998**, *19*, 1639.
18. Case, D. A.; Pearlman, D. A.; Caldwell, J. W.; Cheatham, T. E., III; Wang, J.; Ross, W. S.; Simmerling, C. L.; Darden, T. A.; Merz, K. M.; Stanton, R. V.; Cheng, A. L.; Vincent, J. J.; Crowley, M.; Tsui, V.; Gohlke, H.; Radmer, R. J.; Duan, Y.; Pitera, J.; Massova, I.; Seibel, G. L.; Singh, U. C.; Weiner, P. K.; Kollman, P. A. *AMBER 7*; University of California: San Francisco, CA, USA, 2002.
19. Pearlman, D. A.; Case, D. A.; Caldwell, J. W.; Ross, W. S.; Cheatham, T. E., III; DeBolt, S.; Ferguson, D.; Seibel, G. L.; Kollman, P. A. *Comp. Phys. Commun.* **1995**, *91*, 1.
20. Bressanelli, S.; Tomei, L.; Rey, F. A.; De Francesco, R. *J. Virol.* **2002**, *76*, 3482.
21. Cornell, W. D.; Cieplak, P.; Bayly, C. I.; Gould, I. R.; Merz, K. M.; Ferguson, D. M.; Spellmeyer, D. C.; Fox, T.; Caldwell, J. W.; Kollman, P. A. *J. Am. Chem. Soc.* **1995**, *117*, 5179.
22. Onufriev, A.; Bashford, D.; Case, D. A. *J. Phys. Chem. B* **2000**, *104*, 3712.
23. Feig, M.; Onufriev, A.; Lee, M.; Im, W.; Case, D. A.; Brooks, C. L., III *J. Comput. Chem.* **2004**, *25*, 265.
24. Fermeglia, M.; Ferrone, M.; Pricl, S. *Bioorg. Med. Chem.* **2002**, *10*, 2471.
25. Felluga, F.; Pitacco, G.; Valentin, E.; Coslanich, A.; Fermeglia, M.; Ferrone, M.; Pricl, S. *Tetrahedron: Asymmetry* **2003**, *14*, 3385.
26. Manfredini, S.; Solaroli, N.; Angusti, A.; Nalin, F.; Durini, E.; Vertuani, S.; Pricl, S.; Ferrone, M.; Spadari, S.; Foher, F.; Verri, A.; De Clercq, E.; Balzarini, J. *Antiviral Chem. Chemother.* **2003**, *14*, 183.
27. Metullio, L.; Coslanich, A.; Fermeglia, M.; Ferrone, M.; Fuchs, S.; Paneni, M. S.; Pricl, S. *Biomacromolecules* **2004**, *5*, 1371.
28. Mamolo, M. G.; Zampieri, D.; Vio, L.; Fermeglia, M.; Ferrone, M.; Pricl, S.; Scialino, G.; Banfi, E. *Bioorg. Med. Chem.* **2005**, *13*, 3797.
29. Bayly, C. I.; Cieplak, P.; Cornell, W. D.; Kollman, P. A. *J. Phys. Chem.* **1993**, *97*, 10269.
30. Singh, U. C.; Kollman, P. A. *J. Comput. Chem.* **1984**, *5*, 129.
31. Besler, B. H.; Merz, K. M.; Kollman, P. A. *J. Comput. Chem.* **1990**, *11*, 431.
32. Dewar, M. J. S.; Zoebisch, E. G.; Healy, E. F.; Stewart, J. J. P. *J. Am. Chem. Soc.* **1985**, *107*, 3902.
33. Huo, S.; Wang, J.; Cieplak, P.; Kollman, P. A.; Kuntz, I. D. *J. Med. Chem.* **2002**, *45*, 1412.
34. Wang, J.; Cieplak, P.; Kollman, P. A. *J. Comput. Chem.* **2000**, *21*, 1049.
35. Mehler, E. L.; Solmajer, T. *Protein Eng.* **1991**, *4*, 903.
36. Frecer, V.; Kabelac, M.; De Nardi, P.; Pricl, S.; Miertus, S. *J. Mol. Graph. Model.* **2004**, *22*, 209.
37. Jorgensen, W. L.; Chandrasekhar, J.; Madura, J. D.; Impey, R. W.; Klein, M. L. *J. Chem. Phys.* **1983**, *79*, 926.
38. Berendsen, H. J. C.; Postma, J. P. M.; van Gunsteren, W. F.; DiNola, A.; Haak, J. R. *J. Chem. Phys.* **1984**, *81*, 3684.
39. Ryckaert, J. P.; Ciccotti, G.; Berendsen, H. J. C. *J. Comput. Phys.* **1977**, *23*, 327.
40. Darden, T.; York, D.; Pedersen, L. *J. Chem. Phys.* **1993**, *98*, 10089.
41. Srinivasan, J.; Cheatham, T. E.; Cieplak, P.; Kollman, P. A.; Case, D. A. *J. Am. Chem. Soc.* **1998**, *120*, 9401.
42. Kollman, P. A.; Massova, I.; Reyes, C.; Kuhn, B.; Huo, S.; Chong, L.; Lee, M.; Lee, T.; Duan, Y.; Wang, W.; Donini, O.; Cieplak, P.; Srinivasan, J.; Case, D.; Cheatham, T. E., III *Acc. Chem. Res.* **2000**, *3*, 889.
43. Kuhn, B.; Kollman, P. A. *J. Med. Chem.* **2000**, *43*, 3786.
44. Gilson, M. K.; Sharp, K. A.; Honig, B. H. *J. Comput. Chem.* **1988**, *9*, 327.
45. Sitkoff, D.; Sharp, K. A.; Honig, B. H. *J. Phys. Chem.* **1994**, *98*, 1978.
46. Sanner, M. F.; Olson, A. J.; Spehner, J. C. *Biopolymers* **1996**, *38*, 305.
47. Wilson, E. B.; Decius, J. C.; Cross, P. C. *Molecular Vibrations*; McGraw-Hill: New York, NY, 1995.
48. Pettersen, E. F.; Goddard, T. D.; Huang, C. C.; Couch, G. S.; Greenblatt, D. M.; Meng, E. C.; Ferrin, T. E. *J. Comput. Chem.* **2004**, *25*, 1605.